Chemical Mapping of Nb_2O_5 Catalysts for Hydrodeoxygenaton via XRD-Tomography

Leonardo A. De Campos[1], Kamila Iskhakova[1], Foteini Zormpa[2], Naiara C. Telis[2], Erisa Saraci[2], Jan-Dierk Grunwaldt[1,2], Klaus Raffelt[2], Thomas L. Sheppard[1,3*]

[1]*Institute for Chemical Technology and Polymer Chemistry, KIT, Karlsruhe, Germany.*
[2]*Institute of Catalysis Research & Technology, KIT, Karlsruhe, Germany.*
[3]*Institute of Chemical Technologies and Analytics, TU Wien, Vienna, Austria.*
**thomas.sheppard@tuwien.ac.at*

Abstract

ABSTRACT - Guaiacol hydrodeoxygenation (HDO) was studied using pelletized X-Nb_2O_5 (X = Ru, Ni, Fe) catalysts to explore structure–activity relations under realistic conditions. Catalysts were prepared by calcination, metal impregnation, and reduction before vapor-phase hydrodeoxygenation at 360 °C. Ru catalysts showed initial activation, while NiFe catalysts deactivated over time due to carbon deposition and possible structural changes, confirmed by SEM. XRD-tomography revealed distinct phase distributions in 3D space within the catalyst pellets, including core–shell structures of Ni^0 and $NiNb_2O_6$ influenced by thermal treatment. These structural differences correlated with catalytic activity and selectivity, demonstrating the role of thermal processing and advanced spatial characterization in optimizing pelletized catalysts for biomass upgrading.
Keywords: Hydrodeoxygenation, X-ray Tomography, Biomass, Synchrotron Radiation

Introduction

The persistent global reliance on fossil fuels has intensified the search for sustainable energy alternatives. Among these, the conversion of non-edible biomass into renewable fuels is a promising route to lower carbon emissions and enhance energy security (1–2). A key step in this process is hydrodeoxygenation (HDO), which removes oxygenated groups from biomass-derived molecules. Guaiacol (2-methoxyphenol) is widely used as a model compound for HDO studies due to its defined methoxy and hydroxyl functionalities (2–3). While various supports (e.g., TiO_2, Al_2O_3, SiO_2) and metals (e.g., Ru, Pt, Ni, Fe) have been explored under different conditions (1), most studies rely on powdered/small particle catalysts, whereas industrial processes generally require more complex pelletized forms. The latter introduces structural heterogeneities such as phase distribution of composite materials and binders that may affect performance (3).

This work investigated pelletized X-Nb_2O_5 (X = Ru, Ni, Fe) catalysts for guaiacol HDO using X-ray diffraction tomography (XRD-tomography). This technique enables spatially resolved analysis of phase composition across entire pellets, from synthesis to post-reaction, revealing internal structural evolution in 3D space that conventional XRD cannot capture. By correlating localized crystalline phases with catalytic activity and selectivity, this approach provided insights into catalyst behavior under realistic conditions and supports the development of more efficient pelletized systems for biomass upgrading.

Experimental

Nb_2O_5 pellets (~6 mm, with carbon binder, CBMM, Brazil) were first calcined at 500 °C, then impregnated with $Ni(NO_3)_2$, $Fe(NO_3)_3$, or $RuCl_3$. A second calcination (380–800 °C) was followed by in situ reduction in 10% H_2/N_2: 500 °C for 4 h for $NiFeNb_2O_5$, and 300 °C for 4 h for $RuNb_2O_5$ (heating rate: 4 °C/min). Vapor-phase HDO tests were carried out at 360 °C (WHSV = 0.4 h^{-1}, 25–50 h), using 10 wt% guaiacol in decalin, 30 ml/min N_2 (carrier), and H_2/guaiacol = 8:1 (mol:mol). Products were analyzed online by GC-FID and offline by GC-MS. Sample labels reflect thermal treatment steps, e.g., 500-500-300 indicates calcination / calcination / reduction temperature, while X denotes a step that was skipped. Preliminary characterization included ICP-OES, TPO/TPR-MS, in situ XRD, SEM, and TGA. Post-reaction, pellets from selected conditions (including supports) were analyzed by ex situ XRD-tomography at beamline P07 (DESY, Hamburg-DE).

Results and discussions

ICP-OES analysis confirmed the metal content in the calcined samples: Ru at 0.11 wt%, Fe at 1.17 wt% and Ni at 7.18 wt%, as targeted during impregnation. During activity testing, all catalysts exhibited distinct conversion profiles over time on stream (TOS). As shown in Figure 1, most showed gradual deactivation, except for $RuNb_2O_5$ catalysts 500-380-300 and 500-800-300, which initially showed a drop in conversion within the first 5 h, followed by a steady increase. This behavior was likely due to in situ activation

phenomena such as the reduction of residual surface species or restructuring of metal phases, which enhanced active site availability over time (4–5). These trends suggested dynamic behavior involving redox properties, surface acidity, and oxygen vacancy formation, all of which could evolve during reaction and influence catalytic performance.

For the 500-380-300 sample, incomplete precursor decomposition may have initially limited activity, with gradual surface cleaning under H_2 improving performance. The 500-800-300 catalyst likely went through slow reduction of more stable oxides (RuO_2, B-Nb_2O_5, and M-Nb_2O_5) formed during high-temperature calcination, therefore more slowly exposing active sites. In contrast, 500-500-300 had a stable performance, suggesting that favorable metal-support interactions and active phases were formed prior to reaction. $NiFeNb_2O_5$ catalysts showed declining activity, likely due to sintering, carbon deposition, pore blockage (see Figure 2 for SEM results of $NiFeNb_2O_5$ X-500-500).

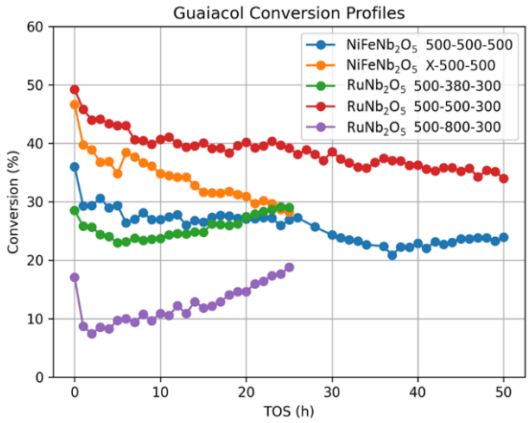

Figure 1. Conversion profiles for different catalysts (25-50 h experiments).

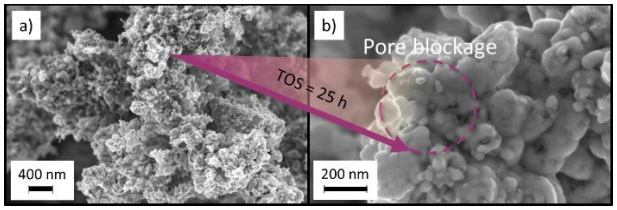

Figure 2. SEM images for $NiFeNb_2O_5$ X-500-500 a) reduced sample (20 kx mag.), b) after reaction (25 h) (80 kx mag.). Coke layer formed indicating pore blockage and catalyst deactivation.

Further insights were obtained through XRD-tomography (Figure 3), which revealed distinct phase distributions within the $NiFeNb_2O_5$ pellets. In the X-500-500 sample, a core-shell structure was observed with metallic Ni^0 concentrated on the shell and $NiNb_2O_6$ dispersed throughout the pellet. The 500-500-500 sample, in contrast, showed the reverse: $NiNb_2O_6$ on the shell and Ni^0 in the core. These differences correlated with catalytic activity and deactivation trends, as selectivity was also influenced by the spatial distribution of active phases. Thermal treatments also affected the carbon binder, likely changing the initial diffusion behavior of metal precursors. At higher temperatures or with multiple calcination steps, binder removal may have tuned precursor impregnation, allowing different distributions of active sites closer to the pellet surface—where they were more accessible during reaction.

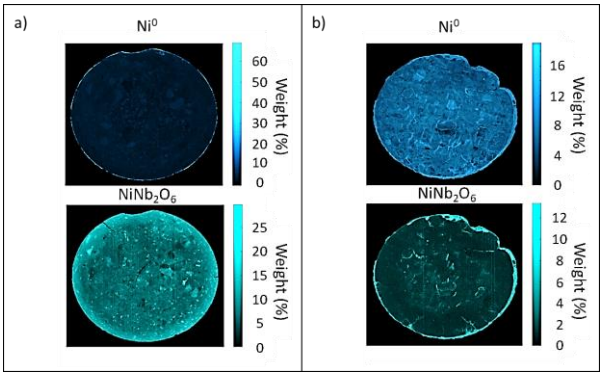

Figure 3. XRD-tomograms for a) $NiFeNb_2O_5$ X-500-500 and b) $NiFeNb_2O_5$ 500-500-500. Ni^0 and $NiNb_2O_6$.

Conclusions

This study shows the potential of X-Nb_2O_5 (X = Ru, Ni, Fe) pelletized catalysts for guaiacol HDO, highlighting how the sequence of thermal treatment influences metal dispersion, structural evolution, and catalytic behavior. Ru-based catalysts revealed initial activation effects for higher and lower calcination temperatures, while NiFe-catalysts suffered from deactivation linked to carbon deposition. Finally, XRD-tomography revealed that the spatial distribution of active sites—such as Ni^0 and $NiNb_2O_6$—demonstrating core-shell structures. These results show the value of advanced structural characterization to understand technical catalyst performance.

Acknowledgements

We acknowledge the German Federal Ministry of Research, Technology and Space (05K22VK4, 13K22VKA).

References

1. G. De Smet; X. Bai; B.U.W. Maes, Chem. Soc. Rev. **2024**, 53, 5489–5551.
2. N.K.G. Silva et al., Fuel **2021**, 287, 119509.
3. J.E. Peters; J.R. Carpenter; C.D. Dayton, Energy Fuels **2015**, 29, 909–916.
4. Q. Chen; H. Xu; H. Li, Sustain. Energy Fuels **2025**, DOI: 10.1039/d5se00544b.
5. K.L. Patle; P. Pardhi; S. Pantawane; D.T. Sarve; J. Ekhe; K.L. Wasewar, Catal. Rev. **2025**, 1–53, DOI: 10.1080/01614940.2025.2453713.